Corrosion Science 100 (2015) 295–305

Contents lists available at ScienceDirect

Corrosion Science

journal homepage: www.elsevier.com/locate/corsci

Quasi-in-situ ex-polarized TEM observation on dissolution of MnS inclusions and metastable pitting of austenitic stainless steel

B. Zhang*,[1], J. Wang[1], B. Wu, Y.T. Zhou, X.L. Ma

Shenyang National Laboratory for Materials Science, Institute of Metal Research, Chinese Academy of Sciences, 110016 Shenyang, China

ARTICLE INFO

Article history:
Received 30 March 2015
Received in revised form 2 August 2015
Accepted 3 August 2015
Available online 5 August 2015

Keywords:
A. Stainless steel
B. STEM
B. Potentiostatic
B. Polarization

ABSTRACT

The pit initiation and growth processes occurring in austenitic stainless steel are included in the passive region of polarization curve. However, polarization measurements do not yield surface morphological insights, which limit the ability to provide a comprehensive picture of the corrosion process. A quasi-in-situ ex-polarized TEM observation method is designed to elucidate the microstructural evolution corresponding to the characteristic regions of the electrochemical polarization curve. This work shows the potential and advantage of combining TEM technique and the traditional electrochemical methods in investigating the initiation of localized corrosion.

1. Introduction

Stainless steels, as typical passive metallic materials, are susceptible to pitting corrosion in the presence of aggressive anionic species. The pitting corrosion of stainless steel is generally believed to originate from the local dissolution of MnS inclusions [1–10]. The dissolution of MnS may involve both electrochemical [2,3,11,12] and chemical dissolution [13] processes in aqueous media. Wranglen [2] proposed a model wherein MnS is primarily electrochemically oxidized to elementary sulfur through the reaction: $MnS = S + Mn^{2+} + 2e$. This model has been further verified by other studies [3,11] in which the sulfur was detected experimentally in neutral solution, albeit via different electrochemical reaction paths. One such path involves the oxidation of MnS to HSO_3^- [3] or $S_2O_3^{2-}$ [11] firstly, and subsequent production of S by cathodic reduction of HSO_3^- or the decomposition of $S_2O_3^{2-}$. Lott and Alkire reported that, thiosulfate was the only product of MnS dissolution in neutral NaCl electrolyte [12]. On the other hand, MnS was found to undergo chemical dissolution at OCP in acidic NaCl solution [13]. Webb et al. [14], through voltammetric response experiment, concluded that MnS inclusions dissolve chemically to HS^- at low anodic potentials under acidic conditions, but dissolve electrochemically at high potentials at neutral pH.

Our previous work using in-situ ex-environmental TEM method [15], gave direct evidence that pitting initiated from the local dissolution of MnS at the interface of the MnS and $MnCr_2O_4$ nano-octahedron embedded in the MnS. The dissolution occurring in the neutral NaCl should be through the electrochemical path as mentioned above. Under anodic polarization, such electrochemical dissolution events of MnS and the subsequent metastable pitting should be reflected in the anodic polarization curve. For austenitic stainless steels, the potentiodynamic polarization curve is typical and representative. Characteristic regions corresponding to active, active–passive, passive and stable pitting events are well known and generally accepted. Observation of corrosion morphologies corresponding to characteristic regions in a polarization curves provide useful insights into some corrosion events reflected in the curve. It is known that pit initiation and metastable pitting, occurring before stable pitting corrosion, overlap the passive region [16,17]. However, the characteristic features indicating pit initiation and metastable pitting in polarization curves are uncertain since polarization curves do not provide information on surface microstructural evolution, e.g., the tiny variation in microstructure resulted from the corrosion process.

Features of the passive region corresponding to the dissolution of MnS inclusions and metastable pitting have been studied using microelectrochemical probe method [9,10,18–23]. Webb

* Corresponding author.
E-mail address: bozhang@imr.ac.cn (B. Zhang).
[1] These authors contributed equally to this work.

http://dx.doi.org/10.1016/j.corsci.2015.08.009
0010-938X/

et al. compared the polarization curves of inclusion-containing and inclusion-free regions and noticed that a steep rise in current was associated with the dissolution of the MnS inclusions [9,22]. Muto et al. [10,23], using a microcell technique combined with SEM and CLSM, observed that MnS dissolution occurred within the passive potential range and attributed the gradual increase in current density and transient current peak appearing within the passive region to the electrochemical dissolution of sulfide inclusions and metastable pitting events, respectively. It is thus obvious that there is as yet no consensus on the microstructural evolution corresponding to characteristic positions in the passive region of polarization curve. This is in spite of extensive studies [16,24–28] focusing on pit nucleation and growth mechanisms using electrochemical noise analysis methods. The corresponding microstructural evolution is undoubtedly necessary to support the electrochemical mechanisms, but this is still lacking due to the difficulty associated with obtaining the microstructural information at the scale dictated by polarization measurements. The present report describes a quasi-in-situ ex-polarized TEM method to investigate microstructural evolution associated with characteristic features of a polarization curve.

2. Experimental procedures

A commercial hot-rolled 316F austenite stainless steel (Nippon Steel and Sumikin Stainless Steel Corporation) was chosen. Compositions (in wt.%) of the 316F steel are given in Table 1. Hot-rolling made the MnS inclusions needle-shaped, and parallel to the rolling direction.

2.1. TEM specimen preparation

The steel rod was first cut into sections of 1 cm using a linear precision saw. Pieces parallel to the rolling direction were sliced with the thickness of 300 μm. The steel piece was ground using grit silicon carbide papers to 120 μm and then was die-cut into disks with diameter of 3 mm. The samples were ground using variant grit silicon carbide papers, polished with diamond paste to 1 μm finish, and finally thinned by ion-milling. After the first-round of TEM observations, some of the specimens were plasma-cleaned and then anodic polarized in NaCl electrolytes at 28 °C. The TEM specimens which underwent electrochemical polarization were quickly cleaned (in distilled water and methanol), dried, and transferred into the TEM for further investigation, designated quasi-in-situ ex-polarized TEM method. A Tecnai G2 F30 transmission electron microscope, equipped with a high-angle angular-dark-field (HAADF) detector and X-ray energy-dispersive spectrometer (EDS) systems, was used at 300 kV in TEM characterization.

2.2. HAADF–STEM imaging technique

HAADF (High Angle Annular Dark Field)–STEM (Scanning Transmission Electron Microscopy) imaging is a newly developed technique in TEM, in which an electron beam (with atomic scale) scans the specimen point to point and an annular detector collects the high-angle scattered electrons (~50 to 200 mrad). The high-angle scattering is predominantly incoherent and roughly proportional to the square of the atomic number, Z, of the scattering atom, which yields HAADF–STEM image [29]. Even small changes in chemical composition and/or thickness are easily distinguished. Therefore this imaging mode has the advantage of studying the initial stage of localized corrosion.

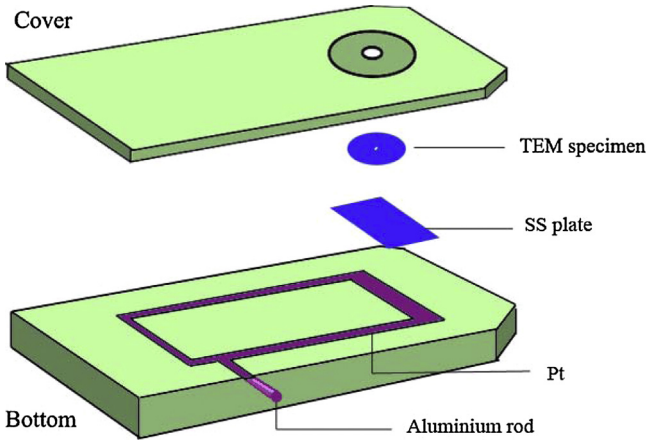

Fig. 1. Schematic diagram of the setup that allows positioning of a TEM specimen as working electrode.

2.3. Electrochemical experiments

In quasi-in-situ ex-polarized TEM observations, obtaining the electrochemical polarization curves of the TEM specimens is key, but quite challenging to accomplish. A traditional three-electrode system was used in electrochemical experiment. The working electrode is the TEM specimen, Pt counter electrode and SCE (saturated with KCl) reference electrode.

A plastic-shelled fixing plate was designed (shown in Fig. 1) to facilitate mounting the TEM specimen as working electrode. The specimen is linked through a Pt slice, which is connected with the outer aluminum rod and fixed by a plastic cover. A 316F stainless steel plate (same material with TEM specimen) is placed between the Pt slice and the TEM specimen in order to avoid electrolyte contact. The specimen was exposed to the electrolyte via the hole in the cover, with diameter 2 mm. Gaps in the setup were coated with thread sealing tape and olefin resin.

It should be noted that all the potential values reported have been normalized with respect to the standard hydrogen electrode (vs. SHE). The electrolyte was NaCl solution with concentrations of 0.5 mol/L and 0.1 mol/L. The electrochemical treatments include potentiodynamic and potentiostatic polarization. In the potentiodynamic polarization measurements, the potential scan began from −250 mV versus OCP and the scan rate was 0.33 mV/s. In the potentiostatic polarization experiments, a potential of 240 mV (vs. SHE) located in the passive region was selected and the current response recorded once every 0.5 s. The electrolytes were maintained at 28 °C with electric-heated thermostatic water bath. The working area of TEM specimen is estimated to be about 0.03 cm^2 and the bulk counterpart is about 0.1 cm^2. AUTOLAB PGSTAT302N electrochemical workstation was used in electrochemical polarization experiments.

3. Results and discussion

3.1. Dissolution of MnS inclusions and metastable pitting under potentiodynamic polarization

A TEM specimen of type 316F stainless steel (316F SS) was polarized in 0.5 mol/L NaCl electrolyte and a potentiodynamic polarization curve was recorded, as shown in Fig. 2a. A polarization curve obtained on a bulk counterpart specimen is also shown in Fig. 2a. The TEM specimen is qualitatively of the same character with the bulk specimen, thus confirming the reliability of the polarization response of the TEM specimen, as well as validating the corresponding microstructural evolution. The polarization measurement was stopped at 345 mV (vs. SHE) below the pit-

Table 1
Compositions of the 316F stainless steel in the present study.

S	C	Cr	Ni	Mn	Mo	Co	V
0.16	0.04	16.68	10.07	1.60	2.15	0.13	0.09
Ti	Cu	Si	P	A1	Nb	Sn	Fe
<0.005	0.26	0.46	0.030	0.06	0.04	0.001	Balance

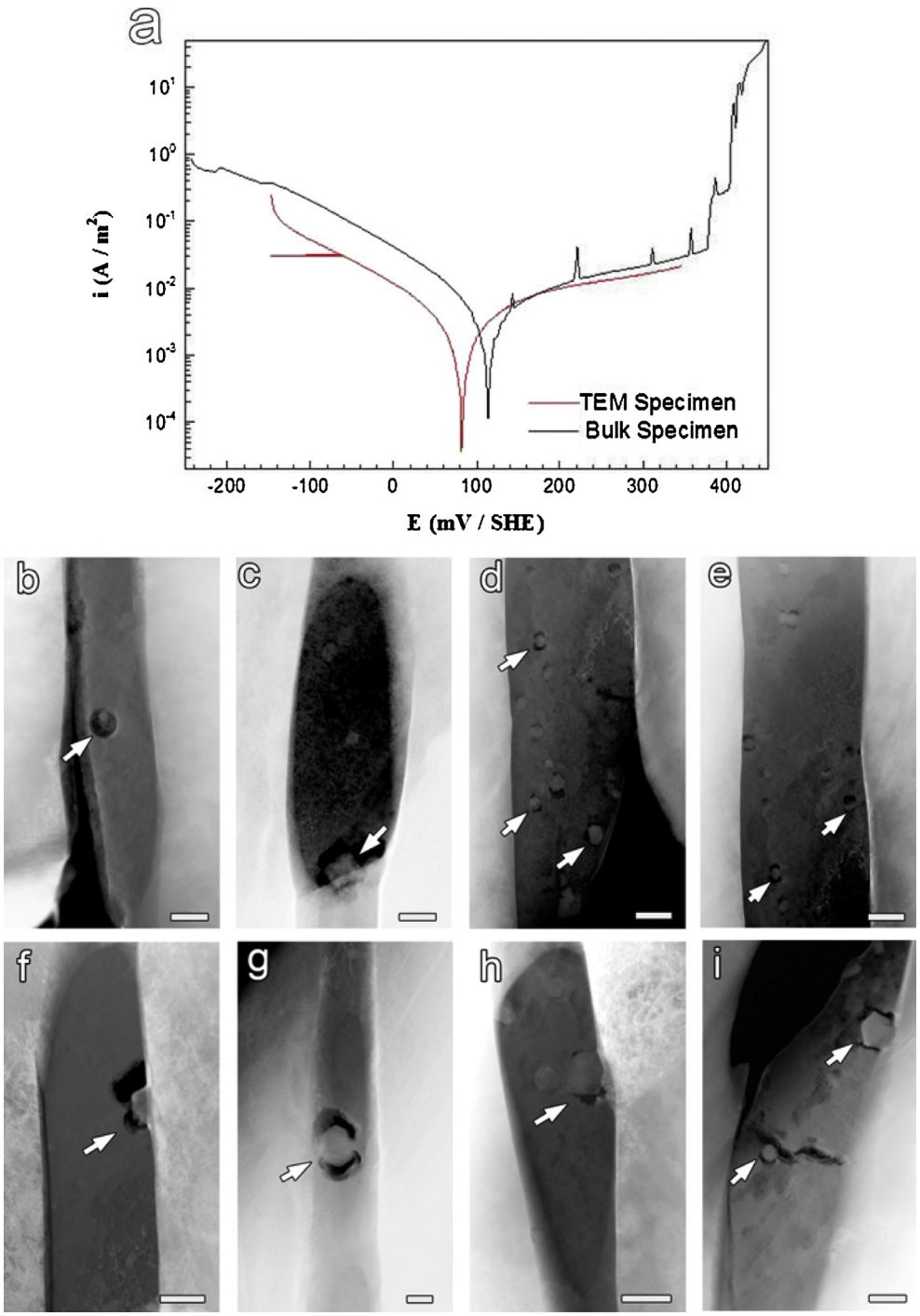

Fig. 2. (a) Potentiodynamic polarization curves measured on bulk and TEM specimens of 316F SS in 0.5 mol/L NaCl and (b–i) HAADF–STEM images (bar = 200 nm) of MnS inclusions after the polarization measurement stopped at 345 mV (vs. SHE).

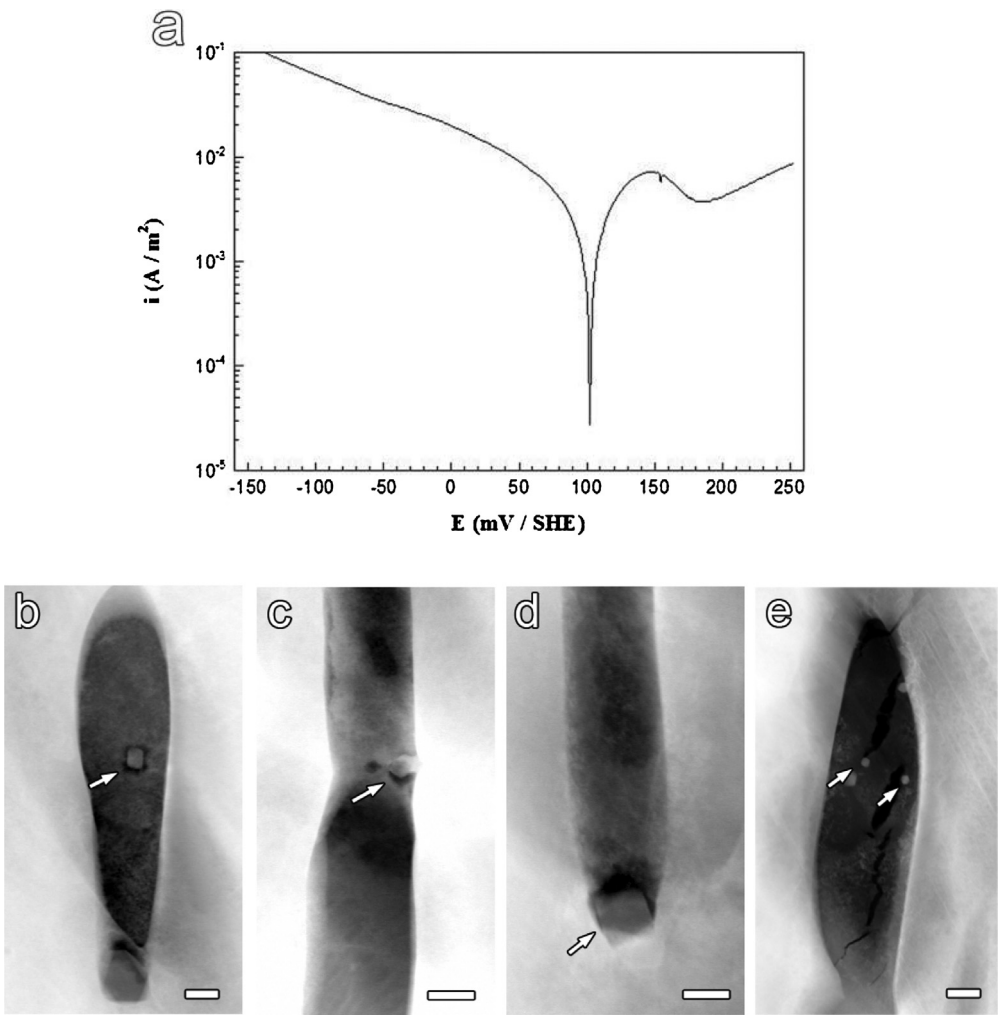

Fig. 3. (a) Potentiodynamic polarization curves measured on TEM specimen of 316F SS in 0.5 mol/L NaCl and (b–e) HAADF–STEM images (bar = 200 nm) of MnS inclusions after the polarization measurement stopped at 250 mV (vs. SHE).

ting potential when the curve was smooth and the anodic current increased slightly with applied potential. The specimen was then observed in a TEM, with particular focus on the microstructural evolution of the MnS inclusions. MnS inclusions with needle shape and the $MnCr_2O_4$ particles embedded in MnS have been identified and characterized in our previous work [11]. All the inclusions in thin zone of the TEM specimen were observed, with the HAADF–STEM images shown in Fig. 2b–i. It can be seen that local dissolution of MnS inclusions occurred at the interface of the MnS and $MnCr_2O_4$ particle. Lowering the end potential to 250 mV (vs. SHE) yields another specimen, with potentiodynamic polarization curve and corresponding structural evolution given in Fig. 3, where the local dissolution is again found in MnS.

A potentiodynamic polarization curve was recorded (Fig. 4a) in 0.1 mol/L NaCl solution and the measurement was stopped once the transient current peaks appeared. Such a specimen was examined and found that the MnS inclusions located within the thin zone had dissolved extensively all over the surface. The thicker zone could not be imaged before polarizing treatment as the electron beam failed to transmit, due to thinning from local corrosive dissolution, nonetheless, the HAADF–STEM images were obtained with good contrast (Fig. 4b–f). It is obvious that the dissolution of inclusions propagated to the stainless steel substrate, forming some pits with diameter 500 nm–2 μm. These pits are metastable pits since their sizes are consistent with those of the metastable pits reported in the literature [10,20,22,30,31]. Some $MnCr_2O_4$ particles were found in metastable pits, which further confirm that $MnCr_2O_4$ particles accelerate pit initiation (i.e., MnS dissolution) and the subsequent propagation process.

Our results provide direct experimental evidence that the gradual increase in current density within the passive region results from the electrochemical dissolution of sulfide inclusions, with transient current peaks originating from the metastable pitting, when the dissolution has propagated to the steel matrix.

3.2. *Local dissolution and propagation in MnS under potentiostatic polarization*

Fig. 5a shows the current response at a potential of 240 mV (vs. SHE) located within the passive potential range in 0.5 mol/L NaCl. The plot shows a steady drop in the current during the interval 0–200 s (Fig. 5a-I) and then a gradual rise after 200 s (Fig. 5a-II). Superimposed onto the background current are a large number of current transients which represent transient breakdown events. The curve includes three current peaks with value of 30–90 nA, two peaks of 20–30 nA and some peaks below 10 nA. Three forms of current transients are identified in such a train of events. The details of the shapes of the current transients are enlarged in Fig. 5a-1 to a-6. The first type is illustrated in Fig. 5a-1 to a-3 and has the shape of a linear rise followed by a linear drop (triangular wave).

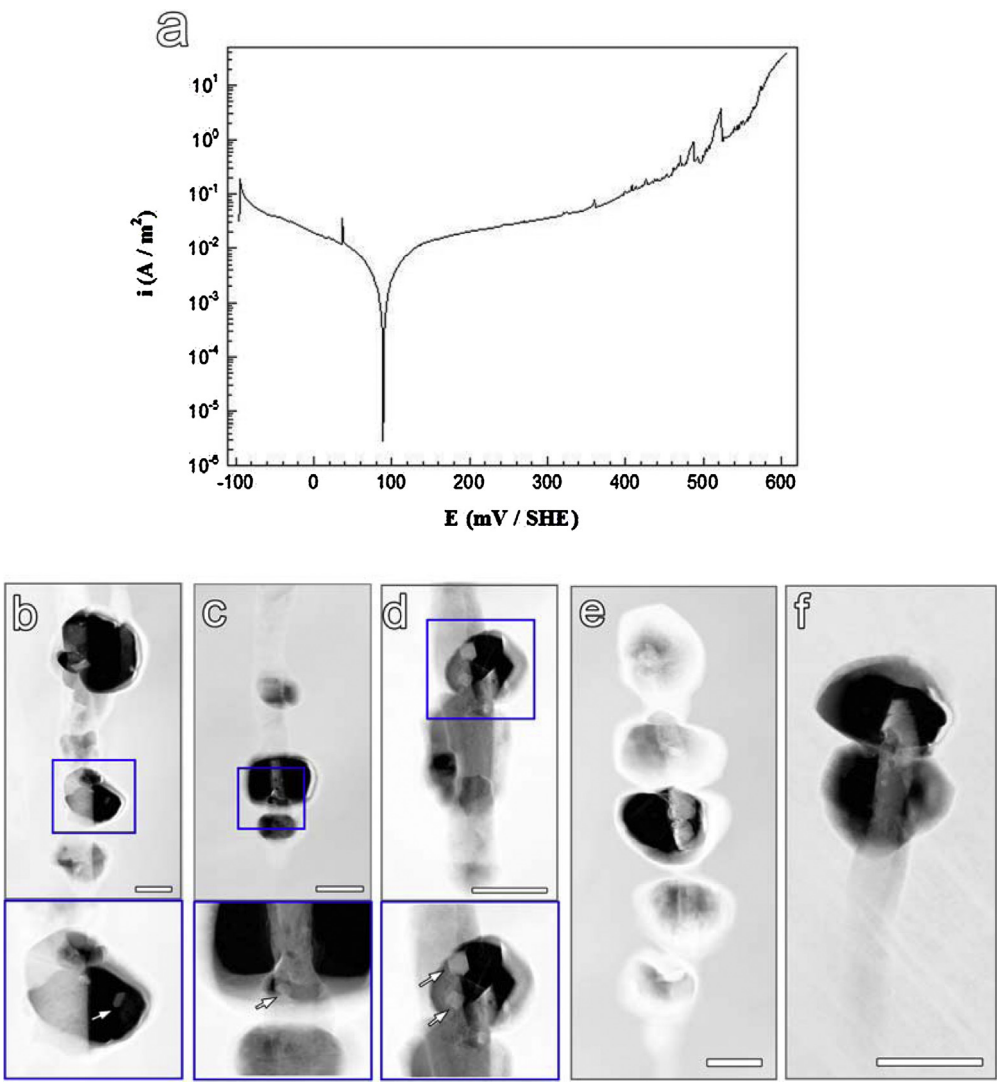

Fig. 4. (a) Potentiodynamic polarization curve measured on TEM specimen of 316F SS in 0.1 mol/L NaCl and (b–f) HAADF–STEM images (bar = 1 μm) of MnS inclusions after the polarization measurement. The measurement was stopped when transient current peaks appeared. The inserts (shown in b–d) are the zoom-in counterparts of the labeled part with rectangle. It is obvious that the dissolution of inclusions has propagated to stainless steel matrix.

Such an event terminates after 1–2 s. The second type of current transients, shown in Fig. 5a-4 and a-5, show a continuous rise followed by a sudden decay. The current does not rise smoothly but increases in several current increments, which is consistent with the reported result [16]. That event continued approximately for 13 s, which is much longer than that of the triangular transients. The third type is shown in Fig. 5a-6 and involves a gentle rise in current followed by a partial decay. After the partial decay, the current continues to rise linearly and then suddenly expires. This event takes about 12 s. It is worthy of note that the first type of current transient is generally found at the initial stages, whereas the other two types are usually observed in the later stage.

The triangular wave form is widely reported to be observed for metals in a passive state [26,28], with the time interval of approximately 1–3 s between the current rise and drop stages. On the other hand, the current transient with the feature of a gentle rise followed by a sudden decay has been widely observed during metastable pitting of various stainless steels [16,24,25,28,32]. The usual exponential rise in current with time corresponds to the pit propagation stage, while the sudden decay is attributable to the repassivation of the pits. The third type of current transients is similar to that reported by Burstein and Mattin [27], which to describe pit propagation proceeded by a nucleation event.

Fig. 5b–e shows the STEM images illustrating the possible corrosion events corresponding to the features of the current transients described above. It is clear that majority of the MnS inclusions dissolved and the local dissolution originate adjacent to $MnCr_2O_4$ particles (only four of them are shown here). Relatively severe dissolution of MnS is illustrated in Fig. 5c and d in which the dissolution has propagated extensively in MnS. Accordingly, the second type of current transients may be ascribed to the propagation of local dissolution in MnS. The next consideration is to account for the triangular transients.

Experiments were also undertaken using a lower concentration of electrolyte (0.1 mol/L NaCl), which is relatively less aggressive and thus allows us to capture more information on initial corrosion processes occurring within the same period of time. Moreover, the frequency of pitting events has been found to decrease with reduction in chloride concentration [17]. A specimen was held at 240 mV (vs. SHE) in 0.1 mol/L NaCl and the polarization was stopped

when only two current peaks with value of 80–90 nA appeared. TEM observation of the specimen was carried out before and after polarization (Fig. 6b-c). A majority of MnS inclusions (shown in Fig. 6b) remained unchanged before and after polarization, and only a few inclusions (shown in Fig. 6c) dissolved locally. A relatively severe dissolution of MnS is obvious in the first image of Fig. 6c. Similarly, another specimen was observed (Fig. 7), corresponding to a potentiostatic polarization curve including two current peaks with value of 6 and 10 nA, and was found that only one of the MnS inclusions suffered slightly local dissolution (Fig. 7d). When polarization was discontinued before appearance of any current peak (as shown in Fig. 8), no local dissolution was observed in the images obtained before and after polarization.

The transient current peaks in Figs. 6 and 7 were enlarged as illustrated in Fig. 6a-1 to a-3 and Fig. 7a-1 to a-2. All the peaks are seen to have the triangular shape. The peak shape in Fig. 7a-1 seems identical with the third type of peak shown in Fig. 5a-6 but possesses distinct features that suggest that the peak is a combination of two triangular peaks. The sole triangular peaks correspond to the local dissolution of MnS occurring adjacent to some $MnCr_2O_4$ particles. The initial dissolution of MnS can be regarded as the pit nucleation process. Thus, one triangular peak represents one nucleation event or many nucleation events occurring simultaneously. Accordingly, the current transient shown in Fig. 7a-1 should represent successive nucleation events. By that analogy, the third type of current transient, with feature of a continuous rise and a partial decay followed by a rise and a sudden decay, describes a dissolution propagation in MnS proceeded by a new dissolution event.

In the present study, the needle shaped MnS inclusions are surrounded by a large number of $MnCr_2O_4$ oxide particles, which trigger the local dissolution of MnS with various activities. At the initial stage, one or more oxides, around the pit nucleation sites trigger the local dissolution of MnS without further propagation. This gives rise to one or several triangular current peaks. The sites adjacent to other oxides remain available for new nucleation, and this can happen repeatedly. The nucleation process proceeds with propagation of dissolution at some sites, resulting in the second type of current transient, with a continuous rise followed by a sudden decay. Certainly, the propagation process will be accompanied by some new nucleation events. Therefore, the triangular shaped current transients are generally found in the initial stage and few are observed in the later stage. Whereas, the second and the third type of peaks correlated with the dissolution propagation process appears mainly in the later stage.

Here, it is worthy to note that the corrosion events highlighted by all the potentiostatic polarization results only correlate with the local dissolution, nucleation and propagation within the interior of the MnS inclusions. So, these events should be categorized as the pit initiation stage, but not as the metastable pitting stage. Metastable pitting proceeds only when the dissolution of MnS propagates to the steel matrix, as shown in Fig. 4b–f.

Apart from the identification of corrosion events from the features of current transients, the sizes and dimensions of the peaks reflect, to a certain extent, the degree of dissolution in the MnS as well as the severity of dissolution, according to the electrochemical results and the corresponding TEM observations above.

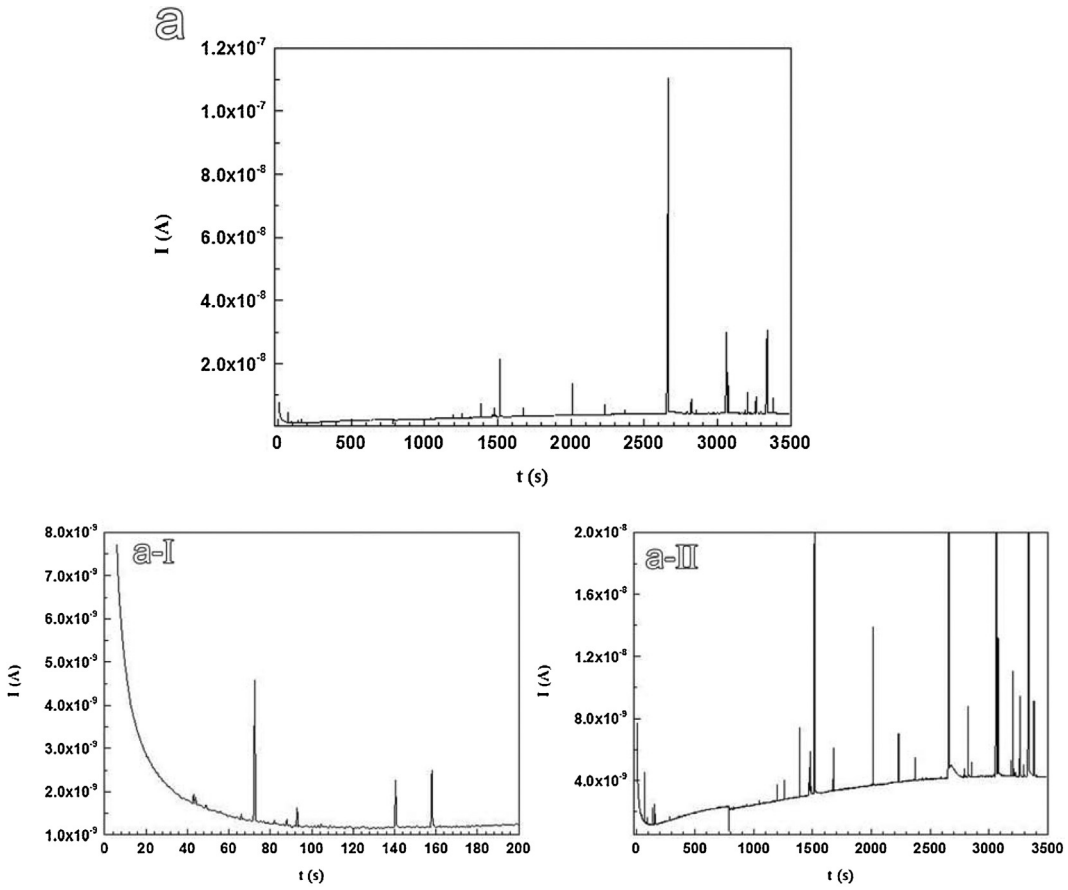

Fig. 5. (a) Current response after the potential was stepped to 240 mV (vs. SHE) for TEM specimen of 316F SS in 0.5 mol/L NaCl and (b–e) HAADF–STEM images (bar = 500 nm) of MnS inclusions after the polarization measurement. (a-II) and (a-II) are the enlarged diagrams corresponding to (a) showing the general trend in the background current. (a-1)–(a-6) are the zoom-in images showing the details of the shape of the current transients.

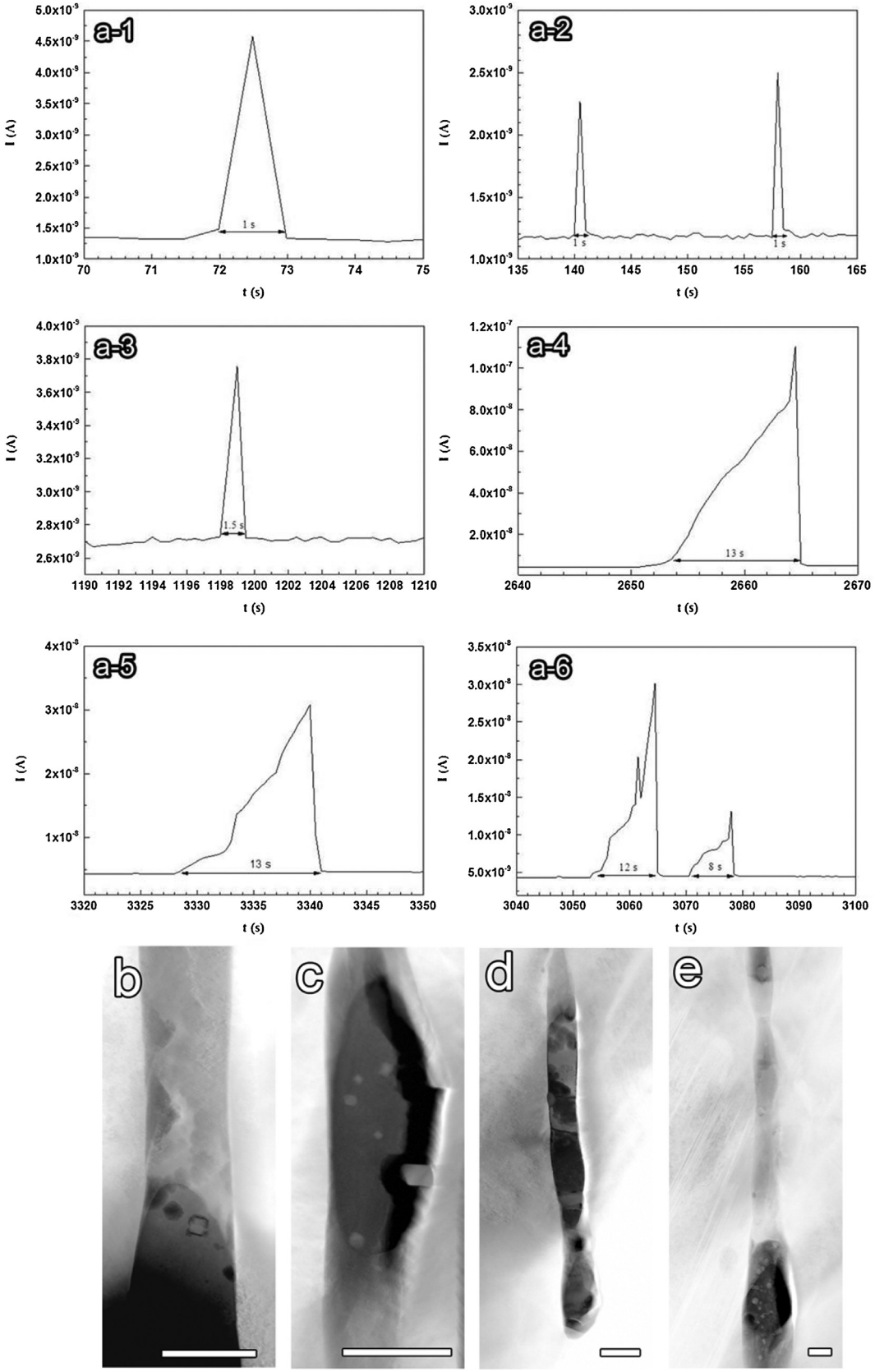

Fig. 5. (*Continued*).

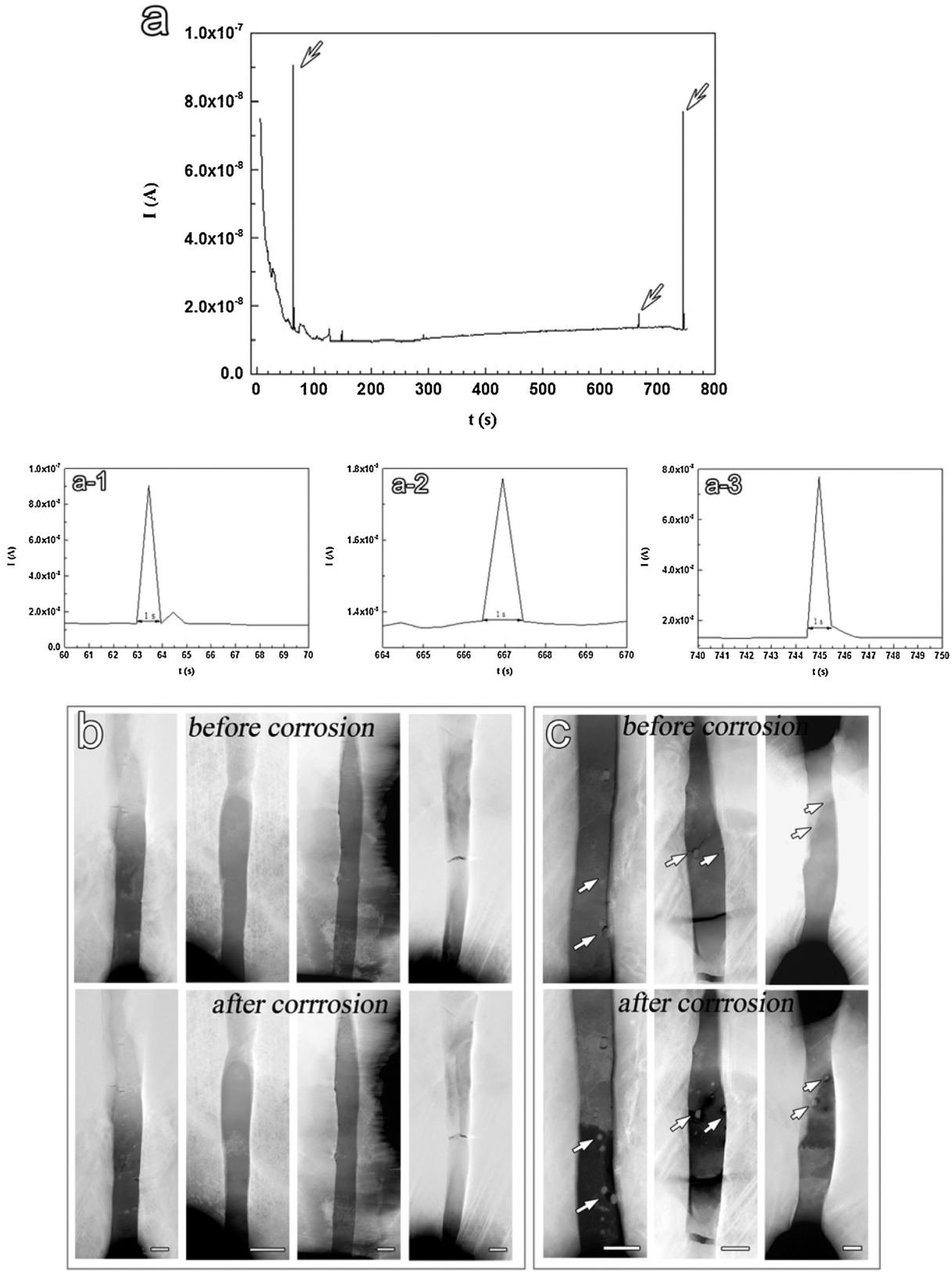

Fig. 6. (a) Current response after the potential was stepped to 240 mV (vs. SHE) for TEM specimen of 316F SS in 0.1 mol/L NaCl. (b–c) HAADF–STEM images (bar = 500 nm) showing MnS inclusions before and after the polarization measurement. (a-1)–(a-3) are the zoom-in images of the arrowed peaks in (a) showing the current transients with feature of triangular shape.

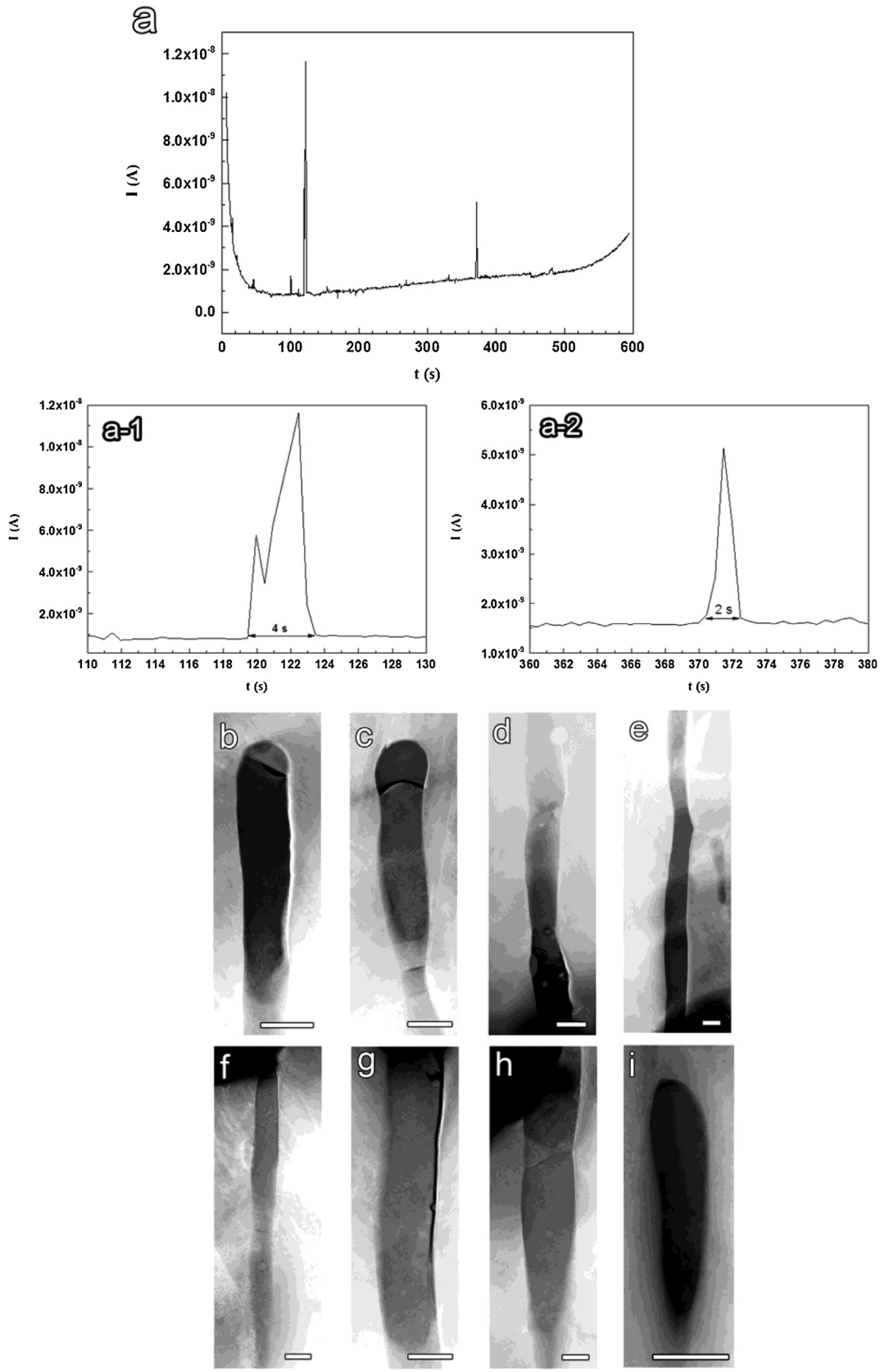

Fig. 7. (a) Current response after the potential was stepped to 240 mV (vs. SHE) for TEM specimen of type 316F SS in 0.1 mol/L NaCl. (b–i) HAADF–STEM images (bar = 500 nm) of MnS inclusions after the polarization measurement. (a-1) and (a-2) are the zoom-in images of the two peaks in (a) showing the current transients with feature of triangular shape.

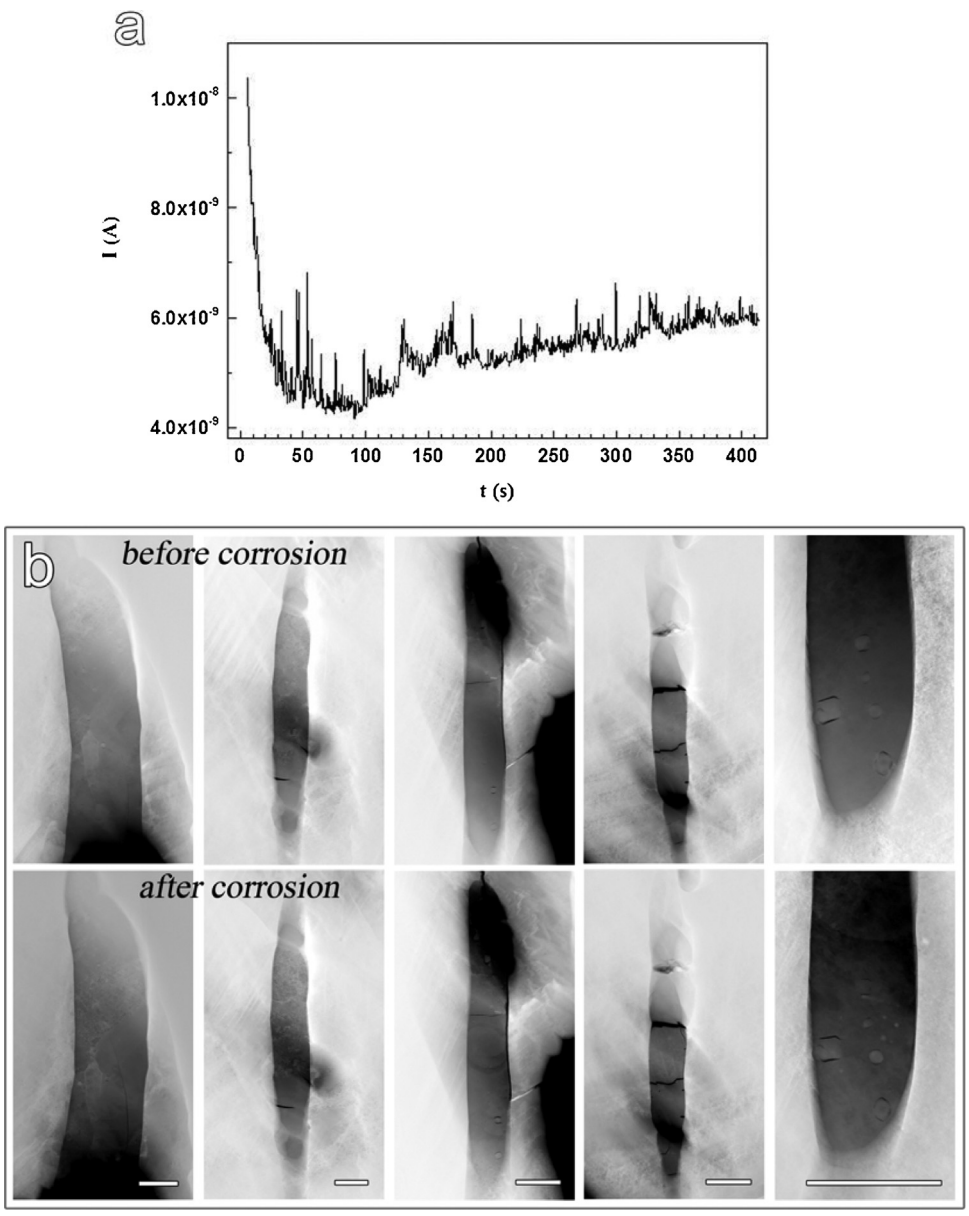

Fig. 8. (a) Current response after the potential was stepped to 240 mV (vs. SHE) for TEM specimen of type 316F SS in 0.1 mol/L NaCl. The measurement was stopped before a transient current peak appeared. (b) HAADF–STEM images (bar = 1 μm) showing MnS inclusions before and after the polarization measurement. It is obvious that no dissolution occurs when no transient current peaks appear.

4. Conclusions

We have applied quasi-in-situ ex-polarized transmission electron microscopy to identify the electrochemical corrosion process underlying the anodic transient current peaks that appear in potentiodynamic and potentiostatic polarization curves. Dissolution of MnS inclusions occur before transient current peaks appear in the passive region of a potentiodynamic curve, corresponding to slight increases in anodic current with applied potential. Transient current peaks in potentiodynamic curves result from metastable pitting events. Similarly, the appearance of current peaks in a potentiostatic polarization curve at a passive potential are correlated with the dissolution of MnS inclusions and the propagation of the dissolution, and the sizes and dimensions of the peaks reflect the quantity of dissolved MnS and the severity of corrosive dissolution.

This work shows the potential and advantage of combining TEM technique and the traditional electrochemical methods in studying the initiation of localized corrosion.

Acknowledgements

This work is supported by the National Natural Science Foundation of China (51101157), the Innovation Fund in IMR and the National Basic Research Program of China (2009CB623705). The authors are grateful to Prof. E.E. Oguzie for suggestion and modification in English.

References

[1] G.S. Eklund, Initiation of pitting at sulfide inclusions in stainless-steel, J. Electrochem. Soc. 121 (1974) 467–473.

[2] G. Wranglen, Pitting and sulfide inclusions in steel, Corros. Sci. 14 (1974) 331–349.
[3] J.E. Castle, R. Ke, Studies by auger-spectroscopy of pit initiation at the site of inclusions in stainless-steel, Corros. Sci. 30 (1990) 409–428.
[4] J. Stewart, D.E. Williams, The initiation of pitting corrosion on austenitic stainless steel: on the role and importance of sulfide inclusions, Corros. Sci. 463 (1992) 457–463, 465-474.
[5] M.A. Baker, J.E. Castle, The initiation of pitting corrosion at mns inclusions, Corros. Sci. 34 (1993) 667–682.
[6] D.E. Williams, T.F. Mohiuddin, Y.Y. Zhu, Elucidation of a trigger mechanism for pitting corrosion of stainless steels using submicron resolution scanning electrochemical and photoelectrochemical microscopy, J. Electrochem. Soc. 145 (1998) 2664–2672.
[7] G.S. Frankel, Pitting corrosion of metals—a review of the critical factors, J. Electrochem. Soc. 145 (1998) 2186–2198.
[8] T. Suter, E.G. Webb, H. Bohni, R.C. Alkire, Pit initiation on stainless steels in 1M NaCl with and without mechanical stress, J. Electrochem. Soc. 148 (2001) B174–B185.
[9] E.G. Webb, R.C. Alkire, Pit initiation at single sulfide inclusions in stainless steel—I. Electrochemical microcell measurements, J. Electrochem. Soc. 149 (2002) B272–B279.
[10] I. Muto, Y. Izumiyama, N. Hara, Microelectrochemical measurements of dissolution of MnS inclusions and morphological observation of metastable and stable pitting on stainless steel, J. Electrochem. Soc. 154 (2007) C439–C444.
[11] A.R.J. Kucernak, R. Peat, D.E. Williams, Dissolution and reaction of sulfide inclusions in stainless steel imaged using scanning laser photoelectrochemical microscopy, J. Electrochem. Soc. 139 (1992) 2337–2340.
[12] S.E. Lott, R.C. Alkire, The role of inclusions on initiation of crevice corrosion of stainless steel—1. Experimental studies, J. Electrochem. Soc. 136 (1989) 973–979.
[13] H. Krawiec, V. Vignal, O. Heintz, R. Oltra, J.M. Olive, Influence of the chemical dissolution of MnS inclusions on the electrochemical behavior of stainless steels, J. Electrochem. Soc. 152 (2005) B213–B219.
[14] E.G. Webb, C.H. Paik, R.C. Alkire, Local detection of dissolved sulfur species from inclusions in stainless steel using Ag microelectrode, Electrochem. Solid-State Lett. 4 (2001) B15–B18.
[15] S.J. Zheng, Y.J. Wang, B. Zhang, Y.L. Zhu, C. Liu, P. Hu, X.L. Ma, Identification of $MnCr_2O_4$ nano-octahedron in catalysing pitting corrosion of austenitic stainless steels, Acta. Mater. 58 (2010) 5070–5085.
[16] P.C. Pistorius, G.T. Burstein, Growth of corrosion pits on stainless steel in chloride solution containing dilute sulfate, Corros. Sci. 33 (1992) 1885–1897.
[17] P.C. Pistorius, G.T. Burstein, Aspects of the effects of electrolyte composition on the occurrence of metastable pitting on stainless steel, Corros. Sci. 36 (1994) 525–538.
[18] V. Vignal, H. Krawiec, O. Heintz, R. Oltra, The use of local electrochemical probes and surface analysis methods to study the electrochemical behaviour and pitting corrosion of stainless steels, Electrochim. Acta 52 (2007) 4994–5001.
[19] T. Suter, H. Böhni, Microelectrodes for corrosion studies in microsystems, Electrochim. Acta 47 (2001) 191–199.
[20] T. Suter, H. Böhni, A new microelectrochemical method to study pit initiation on stainless steels, Electrochim. Acta 42 (1997) 3275–3280.
[21] H. Böhni, T. Suter, A. Schreyer, Microtechniques and nanotechniques to study localized corrosion, Electrochim. Acta 40 (1995) 1361–1368.
[22] E.G. Webb, T. Suter, R.C. Alkire, Microelectrochemical measurements of the dissolution of single MnS inclusions, and the prediction of the critical conditions for pit initiation on stainless steel, J. Electrochem. Soc. 148 (2001) B186–B195.
[23] I. Muto, D. Ito, N. Hara, Microelectrochemical investigation on pit initiation at sulfide and oxide inclusions in type 304 stainless steel, J. Electrochem. Soc. 156 (2009) C55–C61.
[24] C. Gabrielli, F. Huet, M. Keddam, Investigation of electrochemical processes by an electrochemical noise analysis—theoretical and experimental aspects in potentiostatic regime, Electrochim. Acta 31 (1986) 1025–1039.
[25] G.S. Frankel, L. Stockert, F. Hunkeler, H. Boehni, Metastable pitting of stainless steel, Corrosion 43 (1987) 429–436.
[26] A. Legat, V. Dolecek, Corrosion monitoring system based on measurement and analysis of electrochemical noise, Corrosion 51 (1995) 295–300.
[27] G.T. Burstein, S.P. Mattin, The nucleation and early stages of growth of corrosion pits, in: Proceedings of the Symposium on Critical Factors in Localized Corrosion II, The Electrochemical Society, Pennington, NJ, 1996, pp. 1–14.
[28] Y.F. Cheng, J.L. Luo, M. Wilmott, Spectral analysis of electrochemical noise with different transient shapes, Electrochim. Acta 45 (2000) 1763–1771.
[29] S.J. Pennycook, Structure determination through Z-contrast microscopy, in: P.W. Hawkes (Ed.), Advances in Imaging and Electron Physics: Microscopy, Spectroscopy, Holography and Crystallography with Electrons, vol. 123, 2002, pp. 173–206.
[30] R.R. Ke, R. Alkire, Initiation of corrosion pits at inclusions on 304 stainless steel, J. Electrochem. Soc. 142 (1995) 4056–4062.
[31] T. Suter, H. Böhni, Microelectrodes for studies of localized corrosion processes, Electrochim. Acta 43 (1998) 2843–2849.
[32] C. Gabrielli, F. Huet, M. Keddam, R. Oltra, A review of the probabilistic aspects of localized corrosion, Corrosion 46 (1990) 266–278.